THE INFLUENCE OF MODULATED SLOTTED SYNTHETIC JET ON THE BYPASS OF HUMP

Petr Pick*, Miroslav Andrle*, Vladislav Skála*, Milan Matějka*

The articles deals with the influence of phase modulated synthetic jet on the aero-dynamics of the hump in a closed test section of the Eiffel-type wind tunnel. Three experimental methods of measurement techniques of this phenomenon, were used: the pressure profile using the Kiel total pressure probe, the velocity profile using the CTA probe and the visualization of the flow field using the hot film and the thermo camera. The experimental results with and without the influence of the synthetic jet were compared, as well the impact of the phase shift of the neighbouring synthetic jets. As a reference case, the flow around the hump without the influence of the synthetic jet was selected. The results of the measurement are presented in figures and compared.

Keywords : *synthetic jet, Kiel probe, CTA probe, loss coefficient, phase shift, modulation*

1. Introduction

The objective of the article is to verify and visualize the positive influence of the amplitude modulation and the phase shift of the synthetic jet on the flow field behind the hump. The cells of the synthetic jet generator work on their own resonant frequency (the Helmholtz (cavity) frequency) and create vortexes in the flow field which have impact on the size and character of the wake after the hump [1, 3]. Application of synthetic jet with amplitude modulation to the flow reduce pressure and velocity losses – size of wake behind hump [2]. The amplitude and the phase shift of the actuation of neighbouring synthetic jets generators are adjusted to discover the strongest positive effect on the wake size. This effect needs to be analysed. Pressure and velocity measurement techniques were used to verify the influence of the synthetic jet on the flow field behind the hump. Thermal images of the surface of the hump with hot foil were acquired by thermo camera to visualise size of wake.

2. Methods and data

A model of the hump with dimensions $400 \times 300 \times 50$ mm ($L \times W \times H$) was used (figure 1). The model was placed into a channel in an open-circuit wind tunnel with a closed test section (figure 2), the dimension of the cross section area : 300 mm $\times 200$ mm ($L \times W$). The velocity of the free stream in the inlet of the test section area was 8.5 m/s, intensity of turbulence Tu $= 1.1$ %.

Model dimensions are $300 \times 400 \times 50$. Output slots of SJ generator is placed in the location of maximum thickness of the model. Each cell of SJ generator consists of two electrodynamics

* Ing. P. Pick, Bc. M. Andrle, Ing. V. Skála, Ing. M. Matějka, Ph.D., Faculty of Mechanical Engineering at CTU in Prague, Department of Fluid Mechanics and Thermodynamics 12112, Technická 4, Prague
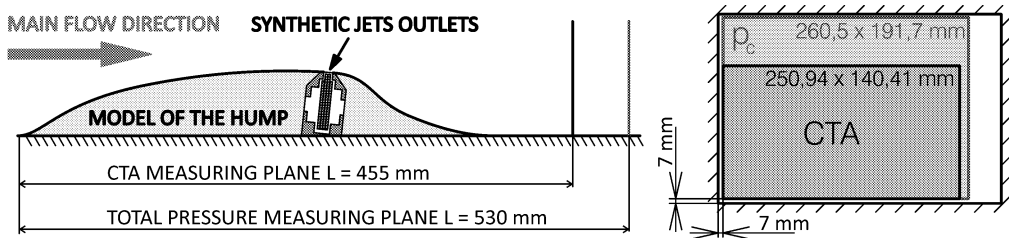
Fig.1: *Model of the hump with synthetic jet (fore-and-aft section), assumed from [1]*
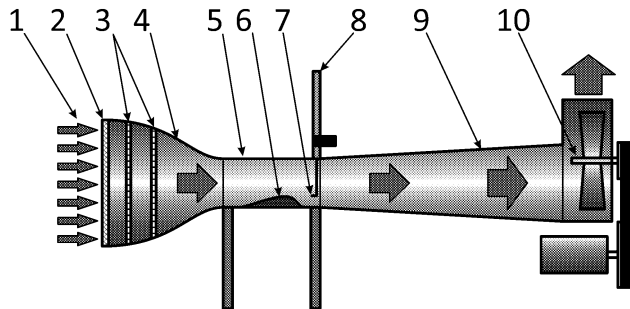

Fig.2: *Schema of the open-circuit wind tunnel with a closed test section, 1 – air intake;*
2 – dust filter; 3 – settling chamber; 4 – contraction cone; 5 – test section;
6 – model; 7 – probe holder; 8 – traversing unit; 9 – diffuser; 10 – drive section
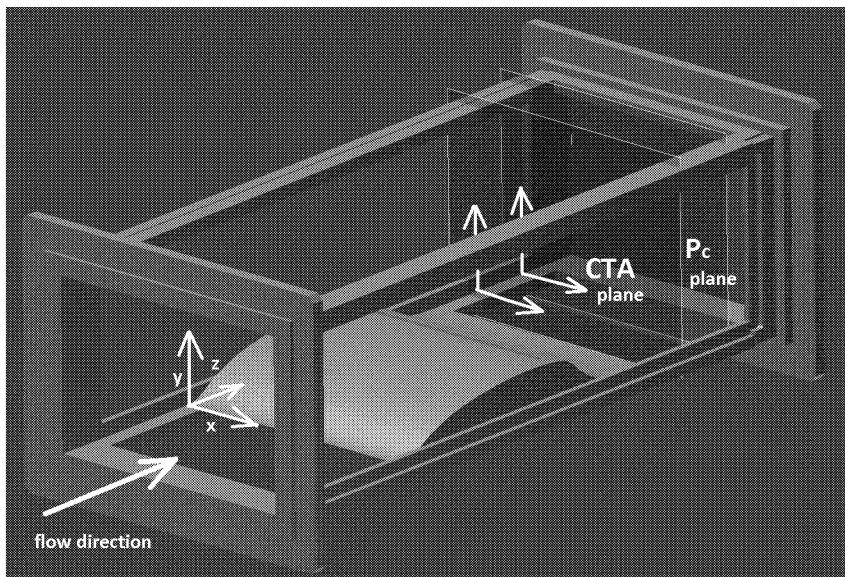

Fig.3: *Coordinate system of model and measurement planes in wind tunnel*

actuators – loudspeakers, mounted in one cavity [4]. The cells are connected in two electric branches, which make it possible to use the phase shift of the actuation of the neighbouring cell's. This phase shift positively influence the flow around the hump in such a way that it will support the generation of the longitudinal vortex structures similar to those being generated by vortex generators [7]. The generator is actuated by a carrier frequency that is identical to

the resonance frequency of cavity (the Helmholtz frequency) and the modulation frequency corresponds to the nondimensional frequency F^+, [6], maximum of free stream energetic spectrum, to reach a maximum efficiency of the flow control with minimal input electric power. Two methods were used to measure the flow field: the total pressure (measured towards atmospheric pressure) measured by the Kiel probe (traversing plane in distance of 530 mm from the leading edge of the model) and the velocity profile measured by the CTA probe (traversing plane in distance of 455 mm from the leading edge of the model), see figure 1 and 3. Size of traversing plane in both cases is smaller due to fixing systems of probes, see figure 1. Starting point (zero point) of traversing plane is situated 7 mm from side and bottom wall of wind tunnel, see figure 4. Influence of the wall on the measurement was small; influence of the boundary layer was more sensitive than influence of near wall thus wall correction wasn't applied. Thermal images using hot foil placed on the surface of hump were captured by thermo camera to visualise the influence of the synthetic jet.

probe type		
Kiel	CTA velocity	Hot foil
no actuation	no actuation	no actuation
actuation 370 Hz carrying f. 60 Hz modulation frequency, 0° phase shift	actuation 370 Hz carrying f. 60 Hz modulation frequency, 0° phase shift	actuation 370 Hz carrying f. 60 Hz modulation frequency, 0° phase shift
actuation 370 Hz carrying f. 60 Hz modulation frequency, 180° phase shift	actuation 370 Hz carrying f. 60 Hz modulation frequency, 180° phase shift	actuation 370 Hz carrying f. 60 Hz modulation frequency, 180° phase shift

Tab.1: List of measured setups at wind tunnel speed 8.5 m/s

2D traversing system controlled by a measuring programme was used. This programme communicates with the stepper motors through an NI PCI-7344 card for stepper drive control and uses an NI PCI-6251 data acquisition card to collect data. For CTA probe measurements, DANTEC miniCTA system with 55P11 probe was used. Traversing by the Kiel and CTA probes was done on a defined traversing grid, respecting the boundary layer, see figure 4. The area marked in the picture by squares was used for measurement with the CTA probe and dots corresponds to measurement with the Kiel probe. The smallest distance between two neighbouring measurement points was about 1.7 mm for the x-axis and 1.4 mm for the y-axis; the greatest distance was 13.1 mm for the x-axis and 14.3 mm for the y-axis.

The picture 4 shows a geometric section by measurement plane; the dots represent the design points of the grid, the squares with dots are the measurement points used for measurements by the CTA probe. For measurements by the Kiel probe, a row of dots above the grid for the CTA probe was added to the grid. This figure also shows the shift of the traversing area against the geometric shape of the test section. The origin of coordinate system of the traversing area is situated on lover left square.

3. Verification of the existence of synthetic jet

Synthetic jet generator was designed with respect to the criteria of existence of the synthetic jet [5], [6] and character of the flow field, [6]. Characteristics of the synthetic jet generator were measured, i.e. the output velocity depending on the input frequencies (carrier and modulation frequency) and the output velocity depending on the input electric
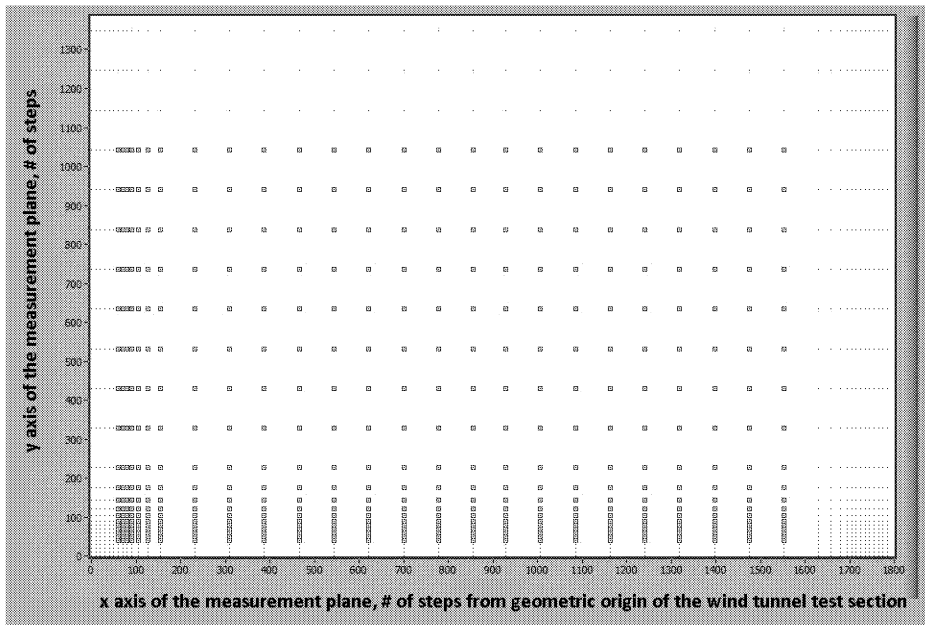
Fig.4: The traversing grid used for measurements by the CTA probe

current. Subsequently the working region of the synthetic jet used in that work was verified. The working region is mentioned in figure 5. ReH is Reynolds number derived by and SH is Stokes number, both derived by [5]. The working region of the designed synthetic jet generator when operating at the carrier frequency of 370 Hz is in a sufficient distance from the border of limit of existence of the synthetic jet. Figure 5 shows the working point for above specified flow velocity in the wind tunnel (8.5 m/s) and the frequency of 370 Hz.
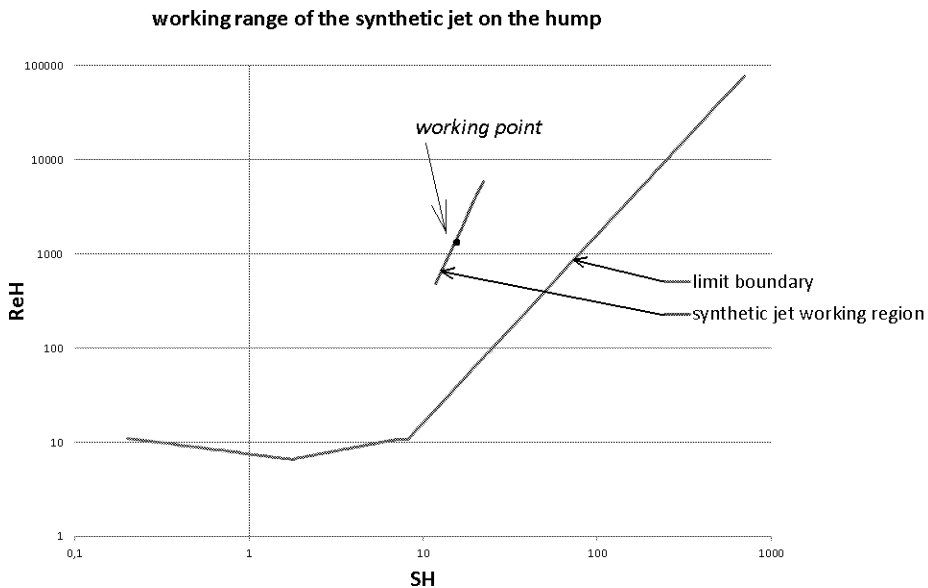
working range of the synthetic jet on the hump

Fig.5: The working region of the synthetic jet generator, ReH is Reynolds number derived by and SH is Stokes number, both derived by [5]

To determine the modulation frequency two processes were used. Estimation of modulation was calculated using nondimensional frequency F^+, $F^+ = f\,X_{\text{te}}/U_\infty$, in more details described in [6]. Data from measured by the CTA probe were used for verification of value of nondimensional frequency. The sampling frequency was $30\,\text{kHz}$, the signal acquisition time was $2\,\text{s}$, and the measurement was carried out in the whole traversing plane defined in Chapter 4. From the acquired data the power spectrum was calculated, see figure 6. The power spectrum, presented in the figure, shows the optimal modulation frequency value by which it is appropriate to influence the flow field, [6]. This optimal frequency is carrying biggest part of energy.
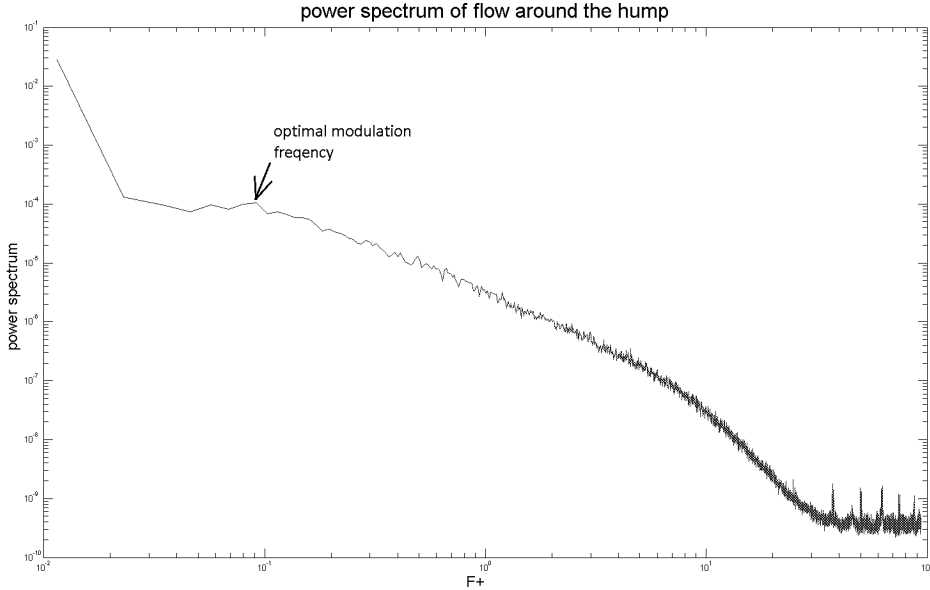

Fig.6: *The power spectrum of the velocity in the 455 mm plane, measured by the CTA probe $F^+ = f_{\text{sj}}\,X_{\text{te}}/U$, where f_{sj} is the frequency of the synthetic jet; X_{te} is the characteristic length corresponding to length of separated area without influence of the synthetic jet; and U is the free stream velocity*

4. Results of the experiment

Three basic experimental conditions were selected in this paper to show the positive influence of phase shift of neighbouring synthetic jets on the flow field. The synthetic jet generator was actuated by carrying frequency $f_{\text{c}} = 370\,\text{Hz}$ and modulation frequency $f_{\text{m}} = 60\,\text{Hz}$. In the one case, there was no phase shift. In the other, the phase shift of amplitude modulation was set in the opposite phase, by $180°$. Dimensions of the area measured by the Kiel probe were $260.5\,\text{mm} \times 191.7\,\text{mm}$. Dimensions measured by the CTA probe were $251\,\text{mm} \times 140.4\,\text{mm}$. The starting points of traversing grid for these measurements were situated near the left bottom corner of the wind tunnel test section ($7\,\text{mm}$ from side and bottom wall of wind tunnel). Therefore, the wall effect of the synthetic jet is not visible on the right side of the wind tunnel. Loss coefficient was defined as follows:

$$\mathrm{d}\xi_{\text{pc}} = \frac{p_{\text{c\,Ref}} - p_{\text{c}}(\text{Kiel})}{p_{\text{d\,Ref}}} \tag{4.1}$$

where $p_{c\,Ref}$ is the reference total pressure in the wind tunnel before the hump, $p_c(\text{Kiel})$ is the total pressure measured by the Kiel probe, $p_{d\,Ref}$ is the reference dynamic pressure before the hump.

For measuring by the CTA probe – mean velocity calculated from measured speed in traversing area is calculate and same for turbulence intensity.

$$u_{\text{RMS}} = \sqrt{\overline{u'(t)^2}} \ ,$$
$$\text{T.I.} = \frac{u_{\text{RMS}}}{\bar{u}} \ .$$

(4.2)

4.1. The Kiel probe results

In figure 7 we can see the total pressure fields in the position of 530 mm from the leading edge. The greyscale represents total pressure measured from reference barometric pressure. In figure 8, the comparison of the total pressure distribution is shown, sections (A) being 0 mm, (B) 62.5 mm and (C) 125 mm from the traversing grid origin. A positive influence of the synthetic jet on the wake size is visible in section B and C, with the phase shift (in C) in particular. The output slot of generator of the synthetic jet starts at about 6 mm from the side of the wall, so the effect of the synthetic jet to the flow field close to side wall cannot be visible. In figure 9 we can see the value of the loss coefficient calculated from the total pressure values. The left-hand graph represents the case with no actuation and the middle graph with an actuation but no phase shift. The right-hand graph represents the case with an active actuation and a phase shift.
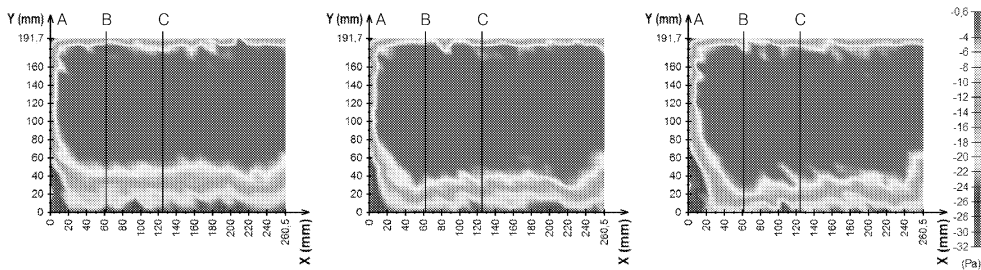

Fig.7: *Total pressure field, view in the direction of the flow; from left: reference conditions – no actuation, no phase shift of the synthetic jet, and phase shift of amplitude modulation of the synthetic jet, the greyscale represents total pressure measured from reference barometric pressure*
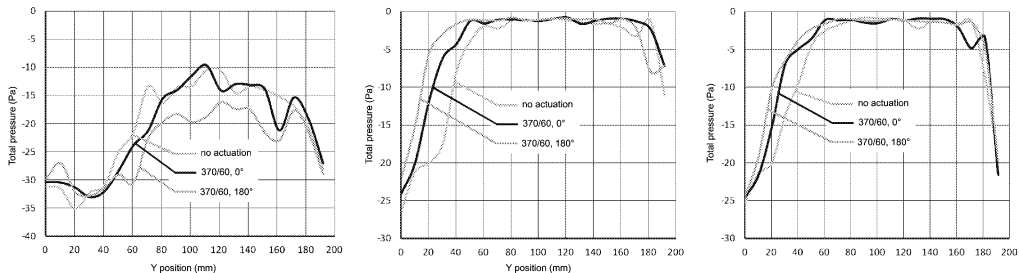

Fig.8: *Comparison of the total pressure distribution in sections, from left: $X = 0\,mm$ (A), $X = 62.5\,mm$ (B), $X = 125\,mm$ (C)*
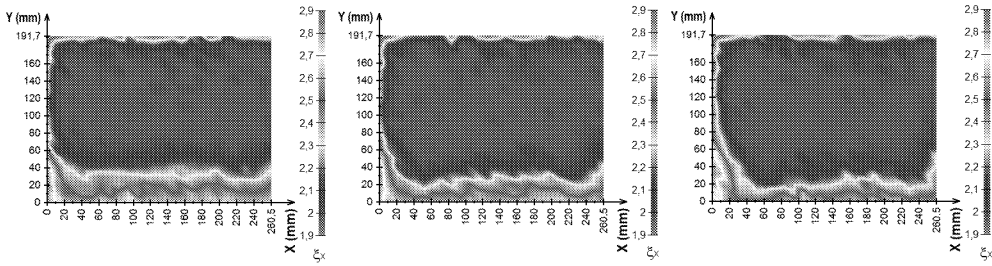
Fig.9: Comparison of the value of the loss coefficient calculated from the measurement by the Kiel probe, from left, the reference conditions are: no actuation, no phase shift of the synthetic jet, and phase shift of amplitude modulation of the synthetic jet

4.2. The CTA probe results

The velocity field measured by the CTA probe is showed in figure 10 (position of 440 mm from the leading edge). Figure 11 shows the comparison of the velocity distribution in sections D, E, F. In figure 12 we can see the turbulence intensity distribution calculated from the values measured by the CTA probe. Results are comparable to the total pressure measurements.
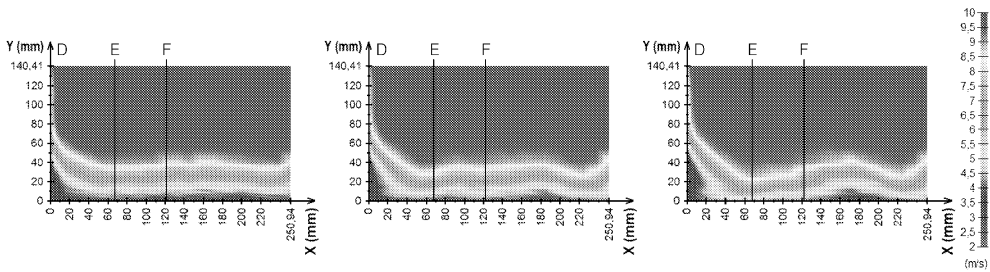

Fig.10: Velocity field, view in the direction of the flow; from left, the reference conditions are: no actuation, no phase shift of the synthetic jet, and phase shift of amplitude modulation of the synthetic jet

Fig.11: Comparison of the velocity distributions in sections D, E, F

4.3. The thermal images

The visualisation of the flow field with the influence of the synthetic jet is showed in figure 13 [8], [9]. The visualisation uses a film heated by a constant heating input and

Fig.12: *The turbulence intensity calculated from the measurement by the CTA probe;*
from left, the reference conditions are: no actuation, no phase shift of the
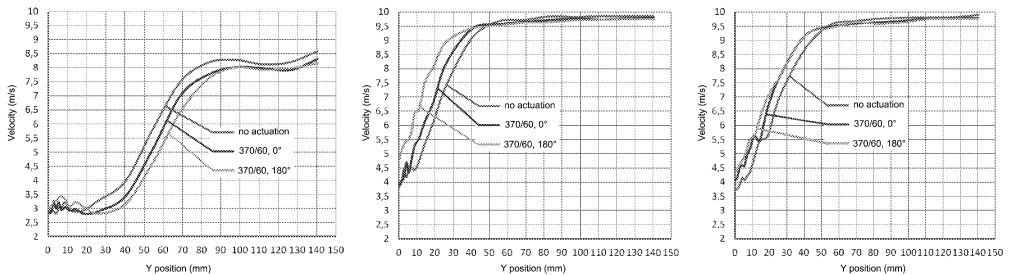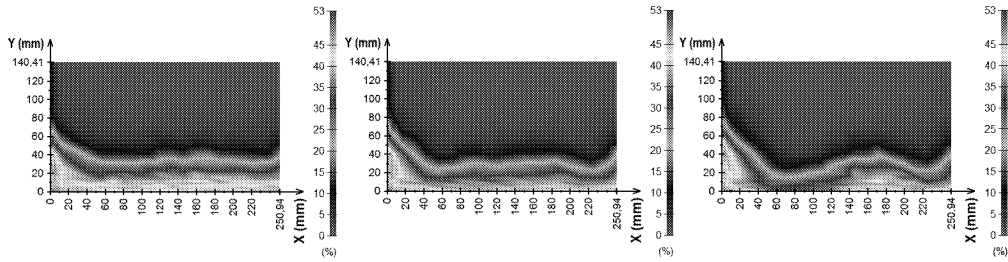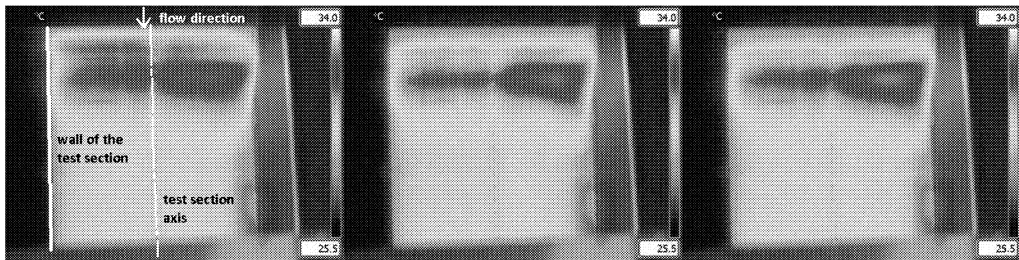*synthetic jet, and phase shift of amplitude modulation of the synthetic jet*

Fig.13: *Temperature field measured on the surface of the hump; from*
left: no actuation, no phase shift of the synthetic jet, and phase
shift of amplitude modulation of the synthetic jet [8], [9]

applied to the surface of the hump. In the case of no actuation, it can be seen in the picture that the high temperature area affects almost the whole first third of the monitored area. This indicates a very early separation of the flow from the model, probably right at its top, where the synthetic jets are located. The heated air stays there for a longer period of time, decreasing the efficiency of the cooling. In cases, where the synthetic jet was activated (without any phase shift and with a phase shift of amplitude modulation), the flow stays on the surface of the model, cooling the film more effectively. The reduction of the high temperature area is smaller close to the wall, because of the effect of side wall of the wind tunnel. It can therefore be concluded that the actuation also had a positive effect on the visualisation of the thermal field. The smaller size of the dark (hot) area indicates a positive effect of the synthetic jet. The smaller dark area corresponds to the smaller size of the recirculation area.

5. Discussion

All methods clearly show a positive influence of the synthetic jet on the flow field around the model. Positive effect of the synthetic jet to the reduction of the wake size is shown in figure 7 and 10. At the bottom of the figure the boundary of the wake is corrugated. This is caused by the influence of the synthetic jet and by the wall effect on the left side of the wall of the wind tunnel. The minimal wake for excitation with phase shift was discovered. In section A, $X = 0$, corner wall effect is considerable and the influence of the synthetic jet is suppressed. For the synthetic jet influence without any phase shift in section A, better results were obtained as far as the corner wall effect is concerned. This is due to the different wake size compared to the effect of the synthetic jet with phase shift. The

mean total pressure in the plane position of $530\,\mathrm{mm}$ (no actuation, no phase shift, phase shift) was $p_{c1} = -7.22 \pm 0.05\,\mathrm{Pa}$, $p_{c2} = -6.45 \pm 0.05\,\mathrm{Pa}$, $p_{c3} = -6.50 \pm 0.05\,\mathrm{Pa}$ (lower value means higher loses). The mean velocity in the plane position (no actuation, no phase shift, phase) was $c_1 = 6.43 \pm 0.03\,\mathrm{m\,s^{-1}}$, $c_2 = 6.54 \pm 0.03\,\mathrm{m\,s^{-1}}$, $c_3 = 6.63 \pm 0.03\,\mathrm{m\,s^{-1}}$. The mean turbulence intensity in the plane position (no actuation, no phase shift, phase) was $T_{i1} = 27.07\,\%$, $T_{i2} = 25.38\,\%$, $T_{i3} = 24.52\,\%$.

In graphs of the loss coefficient an enlargement of the area with a lower loss coefficient is clearly visible. The calculated values are presented in table 2.

	Kiel probe – loss coefficient [–]	CTA probe – velocity [m/s]	CTA probe – turbulence intensity [%]
Reference case – no actuation	2.1466 ± 0.0002	6.43 ± 0.03	27.07 ± 0.01
Actuation without phase shift	2.1263 ± 0.0002	6.54 ± 0.03	25.38 ± 0.01
Actuation with phase shift	2.1236 ± 0.0002	6.63 ± 0.03	24.52 ± 0.01

Tab.2: Comparison of the loss coefficient in measurement plane calculated from
Kiel probe and CTA probe velocity and turbulence intensity

All these values clearly show positive contribution of the opposite phase shift to the decrease of the wake size. The visualization by the thermal camera shows the advantage of the synthetic jet. The thermogram clearly shows positive effect of the synthetic jet.

6. Conclusion

The synthetic jet generator placed on the top of the model of hump definitely has a positive effect to the wake size. This influence was verified by three different measurement techniques. The opposite phase shift of the neighbouring synthetic jet cells in synthetic jet generator has a positive effect on reducing of the wake behind the model.

Acknowledgments

References

[1] Matějka M., Hyhlík T., Skála V.: Effect of synthetic jet with amplitude modulation on the flow field of hump, 22nd International Symposium on Transport Phenomena, Turbulence and Flow Instabilities, Article No. 109, 2011

[2] Matejka M., Pick P., Prochazka P., Nozicka J.: Experimental Study of Influence of Active Methods of Flow Control on the Flow Filed Past Cylinder, Journal of Flow Visualization and Image Processing, vol. 2009, no. 4, p. 353–365, ISSN 1065-3090, 2009

[3] Colliss S., Jjoslin R.D., Seifert A., Theofilis V.: Issues in active flow control: Theory, control, simulation, and experiment, Progress in Aerospace Sciences, Volume 40, Issues 4–5, Pages 237–289, 2004

[4] Uruba V.: On a synthetic jet flow, PAMM, Special Issue: GAMM Annual Meeting 2005, Volume 5, Issue 1, Pages 557–558, 2005

[5] Trávníček Z., Broučková Z., Kordík J.: Formation criterion for synthetic jets at high Stokes numbers, AIAA J. 50 (2012) 2012–2017

[6] Matějka M., Doerffer P., Kurowski M.: Natural vortex shedding frequency and design of synthetic jet generator, 31. setkání kateder mechaniky tekutin a termomechaniky, Mikulov ISBN 978-80-214-4529-1, p. 149–152, 2012

[7] Součková N., Popelka L., Matějka M., Šimurda D.: Effect of vortex generators on flow condi-tions of airfoil with deflected flap, In 21st International Symposium on Transport Phenomena, Kaohsiung City: National Kaohsiung University of Applied Sciences, 2010, S. 16-24. ISBN 978-986-6184-25-3, 2010

[8] Matějka M., Hyhlík T.: Comparison of numerical simulation and flow field visualisation using heat foil. EPJ Web of Conference, Volume 25, 2012, EFM11 – Experimental Fluid Mechanic 11, art. Nr. 01053, ISSN 2100-014X, 2012

[9] Matějka M., Hyhlík T., Skála V.: Effect of synthetic jet with amplitude modulation on the flow field of hump, 22nd International Symposium on Transport Phenomena, S. 1–9, ISBN 978-90-818208-0-6